The effect of temporal aggregation of weather input data on crop growth models' results

L.G.J. van Bussel[a,b*], C. Müller[b,c], H. van Keulen[a,e], F. Ewert[a,d], P.A. Leffelaar[a]

[a]Plant Production Systems Group, Wageningen University, P.O. Box 430, 6700 AK, Wageningen, The Netherlands

[b]Netherlands Environmental Assessment Agency, P.O. Box 303, 3720 AH, Bilthoven, The Netherlands

[c]Potsdam Institute for Climate Impact Research (PIK), P.O. Box 60 12 03, 14412, Potsdam, Germany

[d]University of Bonn, Institute of Crop Science and Resource Conservation, Katzenburgweg 5, 53115 Bonn, Germany

[e]Plant Research International, Wageningen University and Research Centre, P.O. Box 616, 6700 AP Wageningen, The Netherlands

[*]Corresponding author: Tel: +31 (0)317 482536; Fax: +31 (0)317 484892.

E-mail address: Lenny.vanBussel@wur.nl

Abstract

Weather data are essential inputs for crop growth models, which are primarily developed for field level applications using site-specific daily weather data. Daily weather data are often not available, especially when models are applied to large regions and/or for future projections. It is possible to generate daily weather data from aggregated weather data, such as average monthly weather data, e.g. through a linear interpolation method. But, due to the

nonlinearity of many weather-crop relationships, results of simulations using linearly interpolated data will deviate from those with actual (daily) data. The objective of this study was to analyse the sensitivity of different modelling approaches to the temporal resolution of weather input data. We used spring wheat as an example and considered three combinations of summarized and detailed approaches to model leaf area index development and associated radiation interception and biomass productivity, reflecting the typical range of detail in the structure of most models. Models were run with actual weather data and with aggregated weather data from which day-to-day variation had been removed by linear interpolation between monthly averages.
Results from different climatic regions in Europe show that simulated biomass differs between model simulations using actual or aggregated temperature and/or radiation data. In addition, we find a relationship between the sensitivity of an approach to interpolation of input data and the degree of detail in that modelling approach: increasing detail results in higher sensitivity. Moreover, the magnitude of the day-to-day variability in weather conditions affects the results: increasing variability results in stronger differences between model results. Our results have implications for the choice of a specific approach to model a certain process depending on the available temporal resolution of input data.

Keywords: Spring wheat; Weather generation; Temperature; Radiation; Crop growth model; Climate change

1. Introduction

In recent years, crop productivity assessments have extended from the plot and field scale to the regional or even global scale including much longer time horizons (100 years or more), e.g. to study the effects of global climate change on global crop productivity (Ewert, 2004; Leemans, 1997). The only suitable tools for quantitative assessment of future global crop productivity are crop growth models. Early crop growth models mainly concentrated on plot and field scale (Hansen et al., 2006; Monteith, 2000; Van Ittersum et al., 2003) for assessments covering time-horizons of a season or a year. Due to the change in the scale of crop productivity assessments, crop growth models, with varying degree of detail, are increasingly applied at the continental or global scale, for example: LPJmL (Lund Potsdam Jena managed Land; Bondeau et al., 2007), DAYCENT (Stehfest et al., 2007), GEPIC (Liu et al., 2007), GLAM (Challinor et al., 2004), GAEZ (Tubiello and Fischer, 2007), and WOFOST (Reidsma et al., 2009).

If crop growth models are applied at large scales, problems arise with respect to missing input data (Nonhebel, 1994) and lack of parameter values for different regions with regard to e.g. specific cultivar characteristics. Applying models in regions with missing input data or in regions beyond the domain for which they were developed and validated, may lead to unreliable results (Ewert et al., 2005; Irmak et al., 2005).

Field-scale crop growth models are typically based and validated on site-specific daily weather input data. Historical global daily weather data sets are available, see e.g. Sheffield et al. (2006) and Hirabayashi et al. (2008), with

spatial scales of $1° \times 1°$ and $0.5° \times 0.5°$ grid cells, respectively. For climate change scenarios, some global circulation models (GCMs) provide daily weather data (LLNL, 1989), however, GCM performance at this level of temporal detail has hardly been evaluated; posing considerable limitations on the use of daily weather data from GCMs in climate change impact studies. Alternatively, monthly weather data aggregates for climate change scenarios are available from large-scale climate data sets. Missing daily weather data, such as radiation and temperature, can then be generated on the basis of these average monthly weather data (Nonhebel, 1994; Soltani et al., 2004). Conversion from aggregated, monthly data to daily data can be achieved by (a) simple linear interpolation between monthly averages, as e.g. applied in the LPJmL model (Bondeau et al., 2007; Sitch et al., 2003) and the GLAM model (Challinor et al., 2004) or (b) assuming that weather conditions for all days within one month are identical to the monthly averages, as e.g. applied in a global application of DAYCENT (Stehfest et al., 2007). In addition, monthly averages can be disaggregated to daily values using weather generators, such as stochastic weather generators (e.g. applied by Semenov, 2009), parametric weather generators (e.g. applied by Liu et al., 2009), or semi-parametric weather generators (e.g. applied by Apipattanavis et al., 2010).

Crop growth is the result of nonlinear, dynamic relations between weather, soil water and nutrients, management, and specific crop characteristics (Hammer et al., 2002; Hansen et al., 2006; Semenov and Porter, 1995). Some processes, e.g. photosynthesis, show continuous and mainly nonlinear

changes in their rates if temperature changes. Other processes, such as phenological development, show a much more linear change with variation in temperature. Finally, crops also respond to absolute changes in temperature, i.e. if a crop experiences temperatures outside the range of those typically experienced, significant yield losses may be the result (Porter and Semenov, 2005), e.g. a short period of extremely high temperatures near anthesis in wheat can result in a high number of sterile florets (Ferris et al., 1998; Mitchell et al., 1993). These relationships are implemented in crop growth models in various ways, with different levels of abstraction being used.

Generated weather data, based on linear interpolation or on the assumption of identical weather conditions within one month, lack day-to-day variability in weather patterns, e.g. extreme temperatures are eliminated, in contrast to weather data generated by a weather generator. However, weather generators suffer from various shortcomings, such as lack of available observed site-specific daily weather data in order to calibrate the weather generator (stochastic and semi-parametric weather generators) or normal-distributed data (parametric weather generators) (Apipattanavis et al., 2010). Moreover, so far, weather generators have only been tested for specific regions or sites, which leaves doubt about their applicability at the global scale.

Although linear interpolation is a pragmatic method to generate daily weather data at the global scale, its applicability needs to be carefully examined, because of the nonlinear relationships implemented in crop growth models, which can bias model results considerably (Hansen et al., 2006; Nonhebel,

1994; Semenov and Porter, 1995). Especially in regions with high day-to-day weather variability, linearly generated weather data will show substantial deviations from actual weather. Consequently, differences in model results are likely to be largest in regions with high day-to-day variability. As extreme weather events have been projected to occur more frequently in the future (Beniston et al., 2007; Easterling et al., 2000; Salinger et al., 2005), the use of interpolated data will exclude this aspect of climate change from impact studies.

Temporal aggregation of temperature and radiation data will have different effects on different processes considered in crop growth models, as these differ in their sensitivity to temperature and radiation. Moreover, the degree of detail taken into account in modelling specific processes may determine their sensitivity to temporally aggregated data. Our hypothesis is that a detailed model is more sensitive to the use of aggregated data than a more summarized model. A detailed model is defined in this study as a more explanatory model, i.e. a model that contains most of the interactions and elements important for the system. In contrast, a summarized model is in general more descriptive, it often contains simplified representations of the complicated interactions and processes in the system. The difference in sensitivity between detailed and summarized models is expected due to differences in their characteristic times (or reaction rates) and in their number of nonlinear relationships considered. Crop growth models applied at the continental or global scale differ in their level of detail to simulate the various processes of crop growth. Consequently, the use of temporally aggregated

weather data may have different effects on simulation results among global crop growth models.

Therefore, the objective of this study is to examine the sensitivity of crop models with different modelling detail to the temporal resolution of weather input data. This should provide more insight in the up-scaling of important crop growth processes from field to regional level for global applications. We use spring wheat (*Triticum aestivum*) as an example and analyse two important processes, leaf area development, to simulate radiation interception, and biomass productivity. For each process a summarized and a more detailed modelling approach is used. None of the models used here covers damage due to extreme weather events such as heat stress. These impacts on crop yields are of increasing concern due to expected future climate changes (Battisti and Naylor, 2009; Long and Ort, 2010; Soussana et al., 2010) and are likely to be very sensitive to the temporal resolution of input data if included in crop growth models.. To examine the possible impacts, we have tested a simple threshold model with daily observed and monthly aggregated data sets, and discuss the implications for modelling. Consequently, the effects of temporal resolution of input data on results of crop growth models have to be studied, as data aggregation leads to information losses.

Results are presented for nine locations across Europe, to analyse the effects under different climatic conditions. For each location, both fully irrigated and rainfed conditions were considered.

2. Material and Methods

In crop growth models, two processes play an important role in determining biomass dynamics: radiation interception by leaves and utilization of the intercepted radiation to produce biomass via the photosynthesis process (Gabrielle et al., 1998; Monteith, 1977; Van Delden et al., 2001; Yin et al., 2000). In this study we applied three combinations of summarized and detailed approaches to model radiation interception and biomass productivity, reflecting a range of detail in model structure: a summarized biomass productivity approach was combined with a summarized and a detailed leaf area index approach (Figs. 1a and 1b, respectively) and a detailed biomass productivity approach was combined with a summarized leaf area index approach (Fig. 1c). For each biomass productivity approach, a specific water balance was used to simulate effects of water stress. Details of the approaches and water balances used are given below and in the Appendix. Adam et al. (in press) evaluated the different model combinations against observed data for a wide range of climatic conditions under potential growing conditions, using observed daily weather data. They concluded that, after calibration, all three model combinations were able to reproduce observed yields within reasonable limits.

The three model combinations to calculate crop productivity were driven by both actual and interpolated weather data. To quantify the sensitivity, the average relative differences (B_d, %) between total standing biomass at the end of the growing season with interpolated weather data (B_i, g C m^{-2}) and with actual weather data (B_a, g C m^{-2}) over the nine stations were calculated:

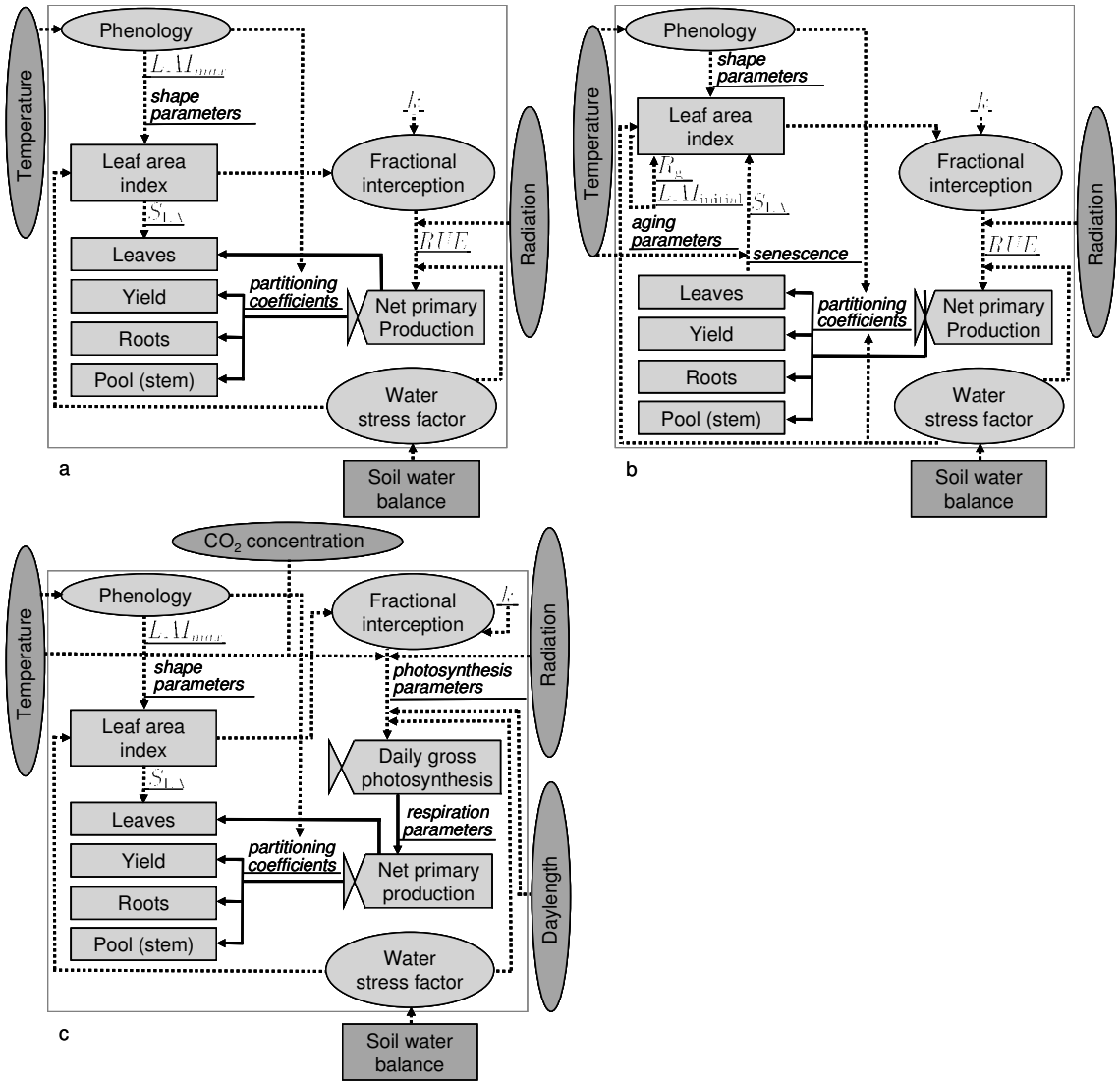

Figure 1: Schematic overview of the different model combinations: a) summarized leaf area index with radiation use efficiency, b) detailed leaf area index with radiation use efficiency, and c) summarized leaf area index with Farquhar photosynthesis.

$$B_{\mathrm{d}} = \sum_{\mathrm{k}=1}^{9} \left| 1 - \frac{B_{\mathrm{i_k}}}{B_{\mathrm{a_k}}} \right| \times \frac{1}{9} \times 100\% \qquad (1)$$

absolute values were used to avoid cancelling out of results.

2.1. Radiation interception

2.1.1. Detailed leaf area index approach

A relatively detailed approach to model leaf area index (LAI, $m^2\ m^{-2}$) dynamics is described by Spitters and Schapendonk (1990) and was applied in the light interception and utilization model (LINTUL) in several case studies of maize (Farré et al., 2000) and potatoes (Spitters and Schapendonk, 1990). Adapted versions of LINTUL (with the same LAI approach, but different assimilation approaches) were used for spring wheat (Ewert et al., 1999; Van Oijen and Ewert, 1999).

Growth of LAI is divided into two phases. During the juvenile stage, or until a certain LAI threshold is reached (LAI_{j}, $m^2\ m^{-2}$), expansion of LAI is exponential. It is governed by temperature through its effect on cell division and extension. If water stress occurs, increase in LAI is reduced by a water stress factor: the ratio between actual and potential transpiration.

Beyond the juvenile stage, LAI expansion is restricted by the supply of assimilates and is calculated using the simulated rate of increase in leaf weight, which is based on the total biomass increment multiplied with a partitioning coefficient, defining the fraction of biomass allocated to the leaves, and with a constant specific leaf area of new leaves (S_{LA}, $m^2\ g\ C^{-1}$). To account for the effect of water stress on LAI beyond the juvenile stage, the increase in leaf weight is reduced through the water stress factor. Leaves die proportionally to their weight with a relative death rate, as a result of self-shading ($R_{\mathrm{d\text{-}sh}}$, d^{-1}) and, in the post-anthesis stage, from aging ($R_{\mathrm{d\text{-}ag}}$, d^{-1}), which is affected by temperature (Fig. 2).

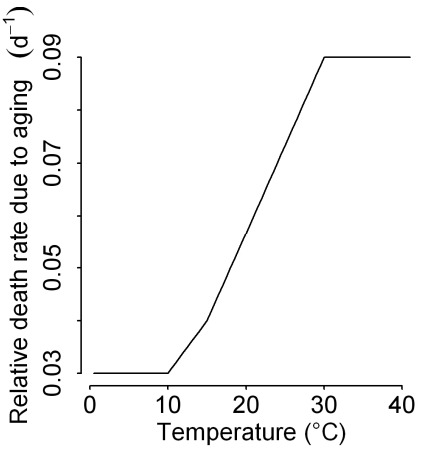

Figure 2: The relative death rate of leaves (d−1) as a function of temperature (°C), as used in the detailed leaf area index approach.

2.1.2. Summarized leaf area index approach

A more summarized approach to model LAI dynamics is based on the concept of the SWAT (Soil and Water Assessment Tool, Neitsch et al., 2005) model and is applied in the LPJmL model. LAI at any point in time is calculated as a fraction of a predefined maximum leaf area index ($LAI_{\max}$, m^2 m^{-2}). This fraction is calculated by a forcing function, defined in terms of sigmoidal and quadratic functions. Potential LAI is reduced if the required biomass to support the calculated LAI is not available.

To account for water stress, in the pre-anthesis phase a water stress factor is included in the rate equation for LAI growth. The water stress factor is either based on the ratio of actual and potential transpiration (in combination with the radiation use efficiency approach), or based on the maximum transpiration rate that can be sustained under optimum soil moisture conditions, soil moisture content, potential canopy conductance, potential evapotranspiration, and a scaling factor (in combination with the Farquhar photosynthesis approach) as described in Sub-section 2.2.1.

The main difference between the two LAI approaches is the strong feedback between biomass production and LAI growth in the detailed LAI approach, while this feedback is weaker in the summarized LAI approach. Growth of LAI in the detailed approach is dependent on so-called allocation factors, i.e. the daily produced biomass is allocated to the different organs in dependence of development stage. Biomass allocated to the leaves is used to calculate LAI using S_{LA}. This implies that, in the detailed approach, unfavourable growing conditions in the beginning of the growing period may have strong effects on final yield levels. A negative feedback may occur: unfavourable growing conditions result in low biomass production, therefore little biomass is allocated to the leaves and this results in low radiation interception, which implies again low biomass production. The effect of unfavourable growing conditions is less strong in the summarized LAI approach, as leaf area is only reduced if water stress occurs or if biomass production is insufficient to sustain the root and leaf biomass (Eq. (A.12)).

2.2. Biomass productivity

2.2.1. Detailed biomass productivity approach

A detailed approach to model biomass productivity is the biochemical photosynthesis model of Farquhar et al. (1980) with simplifications by Collatz et al. (1991). In the process of photosynthesis, CO_2 is converted into carbohydrates through activation of plant enzymes by light. Photosynthesis is either limited by intercepted radiation (J_{e}, g C m^{-2} h^{-1}) or by the availability of the enzyme Rubisco (J_{c}, g C m^{-2} h^{-1}). Intercepted radiation is computed from

current LAI and a constant light extinction coefficient (k, –), using Beer's law. Daily gross photosynthesis is the gradual transition between the two limiting rates and is influenced by ambient temperature, CO_2 concentration, and radiation intensities. Daily net photosynthesis (A_{nd}, g C m^{-2} d^{-1}) is calculated as daily gross photosynthesis minus the "dark" respiration (R_{d}, g C m^{-2} d^{-1}); Figure 3 shows the effect of temperature on daily net photosynthesis for a number of (constant) radiation intensities and a (constant) CO_2 concentration of 350 ppm by volume.

To calculate daily net primary productivity (NPP, g C m^{-2} d^{-1}), maintenance respiration is subtracted from daily net photosynthesis, based on tissue-specific C:N ratios, temperature, and the amount of biomass per organ. The remainder is reduced by 25% to account for growth respiration.

In case of water stress, the model simulates a limited opening of the stomata, causing a change in ratio between intercellular and ambient CO_2 concentrations, which results in a reduced photosynthetic rate (Gerten et al., 2004; Haxeltine and Prentice, 1996; Sitch et al., 2003). Water available for the crop is calculated through a water balance, in which the soil is represented by a simple bucket, containing two layers, each with a fixed thickness. Water content of both layers is updated daily, taking into account transpiration, evaporation, runoff, and percolation through the layers (for more details, see Gerten et al., 2004 and the Appendix).

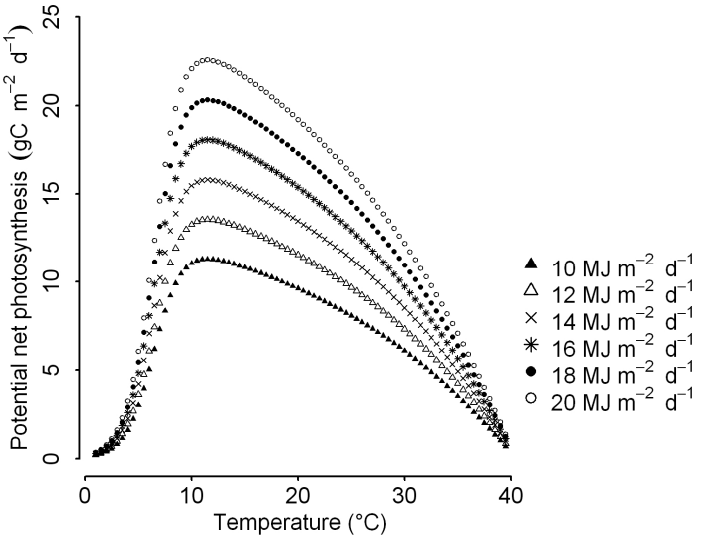

Figure 3: Temperature response of the daily net rate of photosynthesis, at an ambient CO_2 concentration of 350 ppm and various radiation intensities, as simulated with Farquhar photosynthesis.

2.2.2. Summarized biomass productivity approach

A more summarized approach to model biomass productivity is the radiation use efficiency (RUE, g C MJ^{-1}) approach. For crops, a linear relation exists between accumulated intercepted radiation and accumulated biomass, the slope representing the RUE value (Monteith, 1977), which combines the effects of photosynthesis and respiration (Goudriaan and Monteith, 1990). The daily fraction of intercepted radiation by the crop is computed from current LAI and a constant light extinction coefficient, using Beer's law. Daily net primary productivity (NPP, g C m^{-2} d^{-1}) is calculated by multiplying the fraction of intercepted radiation with: daily incoming short-wave radiation (R_{dr}, MJ m^{-2} d^{-1}), 0.5 (to convert short-wave radiation into photosynthetically active radiation), and radiation use efficiency (Eq. (A.34)).

In the absence of water stress, radiation use efficiency is constant; with water stress, it is reduced by the ratio of actual and potential transpiration. Water

available for the crop is calculated through a water balance, in which the soil is represented by a simple bucket, consisting of single layer that increases in thickness in downward direction with the growing roots. Water content of the layer is updated daily, taking into account transpiration, evaporation, runoff, and percolation through the layer (for more details, see Farré et al., 2000 and the Appendix).

The main difference between the two biomass productivity approaches is the dependence of the detailed approach on incoming radiation, CO_2 concentration, and temperature, while biomass productivity calculated according to the summarized approach is only dependent on incoming radiation. Furthermore, the detailed approach includes a coupled photosynthesis-water balance scheme, which allows for accounting for changes in water use efficiency, under changing temperatures or at higher CO_2 concentrations.

Table 1 shows the location-specific (phenological) crop parameters; other crop parameters with regard to radiation interception and biomass productivity are kept constant across the locations (Table 2).

Table 1: Location-specific crop phenological parameters. Source: (Boons - Prins et al., 1993), assuming that sowing dates and temperature sums until maturity of spring barley are representative for spring wheat.

Location (country, latitude (°), longitude (°))	Day of emergence (day of year)	Temperature sum until anthesis (°Cd)	Temperature sum until maturity (°Cd)
UK (52°21′, –0°07′)	56	1185	1693
Denmark (57°06′, 9°51′)	95	1104	1577
The Netherlands (52°06′, 5°10′)	85	1347	1924
Germany (48°07′, 11°42′)	91	968	1383
France (centre) (47°58′, 1°45′)	69	1160	1657
France (south) (43°37′,	41	1504	2149

1°22′)			
Spain (centre) (40°27′,–3°33′)	36	1470	2022
Spain (south) (37°25′, –5°52′)	36	1540	2200
Italy (42°25′, 14°12′)	36	1431	2044

Table 2: Most important parameters for the different model approaches and their values. Sources: (a) (Kiniry et al., 1995), (b) (Van Keulen and Seligman, 1987), (c) (Haxeltine and Prentice, 1996), (d) (Sitch et al., 2003), (e) (Gerten et al., 2004)

Symbol	Parameter	Value and unit	
Parameters for the summarized leaf area index approach			
$fLAI_1$ and $fLAI_2$	Fraction of leaf area index at the first and second inflexion points on the leaf area development curve	0.05 and 0.95 (–)	
fT_{sum1} and fT_{sum2}	Fraction of temperature sum at the first and second inflexion points on the leaf area development curve	0.05 and 0.45 (–)	
$fT_{\mathrm{sum\ a}}$	Fraction of the total temperature sum when anthesis is reached and senescence starts	0.70 (–)	
S_{LA}	Specific leaf area of leaves	0.053 m2 (g C)–1	
LAI_{max}	Maximum leaf area index	5.0 m2 m–2	
Parameters for the detailed leaf area index approach			
R_{g}	Maximum relative growth rate of leaf area index	0.0108 (°Cd)–1	
LAI_{i}	Initial leaf area index	0.025 m2 m–2	
fT_{j}	Fraction of temperature sum when juvenile stage ends	0.15 (–)	
$fT_{\mathrm{sum\ a}}$	Fraction of temperature sum when anthesis starts	0.70 (–)	
LAI_{j}	Threshold leaf area index when juvenile stage ends	0.75 m2 m–2	
T_{base}	Base temperature	0 °C	(a)*
S_{LA}	Specific leaf area of leaves	0.053 m2 (g C)–1	
$R_{\mathrm{d\text{-}shmx}}$	Maximum death rate due to shading	0.03 d–1	(b)
LAI_{c}	Critical leaf area index above which self-shading is assumed to start	4.0 m2 m–2	(b)
Parameters for the radiation use efficiency approach			
RUE	Radiation use efficiency based on total daily radiation	1.38 gC MJ–1	
k	Light extinction coefficient	0.5 (–)	(c)
Parameters for Farquhar photosynthesis approach (C3 plants)			
K_{25} and Q_{10}	The value of the parameter at 25 °C and the relative change in the parameter for a 10 °C change in temperature, respectively		
K_C K_O τ	Michaelis constant for CO2 Michaelis constant for O2 CO2/O2 specific ratio	30 Pa (Q_{10}= 2.1) 30 × 103 Pa (Q_{10}= 1.2) 2600 µmol µmol–1 (Q_{10}= 0.57)	(c)
α_{C3}	C3 quantum efficiency	0.08 µmol µmol–1	(c)
b_{C3}	R_d/V_m ratio for C3 plants	0.015 (gC m–2 d–1) / (gC m–2 d–1)	(c)
λ_{mC3}	Optimal C_i/C_a for C3 plants.	0.8 Pa Pa–1	(d)
P	Atmospheric pressure	100 × 103 Pa	(c)
O_2	Partial pressure of O2	20.9 × 103 Pa	(c)
C_{mass}	Molar mass of carbon	12 gC mol–1	

k	Light extinction coefficient	0.5 (–)	(c)
C_{q}	Conversion factor for solar radiation at 550 nm from MJ m–2 d–1 to mol photons m–2 d–1	4.6 ×10–3 mol photons MJ-1	
c_{a}	Ambient mole fraction CO2	µmol mol–1	
θ	Co-limitation parameter	0.7 (–)	(c)
$\alpha_{\max}$	Maximum Priestley-Taylor coefficient	1.391 (–)	(e)
g_{m}	Scaling conductance	3.26 mm s-1	(e)
$g_{\min}$	Minimum canopy conductance, which accounts for water stress not directly related with photosynthesis	0.5 mm s-1	(e)

2.3. Weather data

Weather input data for the model runs were extracted from a database described by Van Kraalingen et al. (1991), for various locations in Europe (Fig. 4), for the year 1982. It contains daily data for minimum and maximum temperature ($T_{\min}$, $T_{\max}$, ℃), daily incoming short-wave radiation (R_{dr}, MJ m^{-2} d^{-1}), daily precipitation (P, mm d^{-1}), vapour pressure (e, kPa), and wind speed (u, m s^{-1}). Daily average temperature (T_{average}, ℃), used in the radiation interception and biomass production approaches, is calculated from minimum and maximum temperatures.

Data were used from various European weather stations (see Table 1).

Figure 4: Locations of the nine weather stations used in this study.

We concentrated in this study on the effects of linear interpolation of temperature and radiation data only, as effects of disaggregation of precipitation data strongly depend on the soil-water model considered. We here focus on crop growth processes only and do not compare different levels of detail in soil-water models, that would allow addressing the effects of disaggregating precipitation data. Besides, monthly precipitation is mostly disaggregated to daily values in crop growth models on the basis of precipitation generators rather than through linear interpolation (e.g. Bondeau et al., 2007; Liu et al., 2007). Therefore, precipitation is given as daily values in all simulations.

2.3.1. Linear interpolation of temperature and radiation data

Actual daily temperature and radiation values from the nine weather stations were used to derive interpolated daily values for temperature and radiation. Average monthly values, which were assigned to the middle of each month (e.g. $MD_{i=1}$ = 15 and $MD_{i=2}$ = 46), were calculated from the actual weather data. Interpolated daily values for weather variable at day k (X_k, °C or MJ m^{-2} d^{-1}) were calculated as:

$$X_k = X_i + \frac{DOY_k - MD_i}{MD_{i+1} - MD_i} \times (X_{i+1} - X_i) \quad (2)$$

where, X_i and X_{i+1} are monthly averages of weather variable X (°C or MJ m^{-2} d^{-1}) at the middle day of month MD_i and MD_{i+1}, respectively, and DOY_k is the k^{th} day of the year (Sitch et al., 2003; Soltani et al., 2004). The same procedure was applied to derive interpolated daily T_{max} values (°C).

As a measure for the day-to-day variability in weather conditions, the average annual difference (for temperature or radiation) (W_{d}, ℃ or MJ m^{-2} d^{-1}) between linearly interpolated data (W_{i}, ℃ or MJ m^{-2} d^{-1}) and actual data (W_{a}, ℃ or MJ m^{-2} d^{-1}) was computed:

$$W_{\mathrm{d}} = \sum_{\mathrm{k}=1}^{365} |W_{\mathrm{i_k}} - W_{\mathrm{a_k}}| \times \frac{1}{365} \quad (3)$$

A larger difference indicates larger day-to-day variability.

2.3.2. Occurrence of high temperatures

Extremely high temperatures may strongly influence yields through their effects on grain set, since harmful effects occur already after exposure to high temperatures for durations as short as one day (Saini and Aspinall, 1982). In line with a study by Semenov (2009), we summed the number of days with a daily maximum temperature exceeding 27℃ and 31℃ during the ten days after anthesis; two threshold temperatures were used, as wheat cultivars differ in their tolerance to extreme temperatures (Mitchell et al., 1993; Porter and Gawith, 1999). Anthesis was defined as a fixed fraction (0.7) of the temperature sum till maturity (Table 1). Days were summed for the nine locations, based on the data-sets with 1) actual daily T_{max}, 2) interpolated daily T_{max}, 3) actual daily T_{average}, and 4) interpolated daily T_{average}.

3. Results

3.1. Weather data

Day-to-day variability in weather conditions was calculated in order to examine its correlation with possible differences between model results due to the use of input data with different temporal resolutions. Among the

considered study locations, day-to-day variability in weather conditions was highest in Germany and lowest in southern Spain (Fig. 5 and Table 3). Day-to-day variability in weather conditions in Denmark, the Netherlands, France, and the United Kingdom was comparable to that in Germany, while variability in Italy and in central Spain was comparable to that in southern Spain (Table 3).

Table 3: Day-to-day variability in weather conditions.

Location	Average annual deviation between actual and average temperature (℃)	Average annual deviation between actual and average radiation (MJ m-2)
UK	2.22	3.12
Denmark	2.19	3.15
The Netherlands	2.28	3.13
Germany	2.61	3.42
France (centre)	2.40	3.16
France (south)	2.19	3.22
Spain (centre)	1.80	2.68
Spain (south)	1.66	2.30
Italy	1.80	2.71

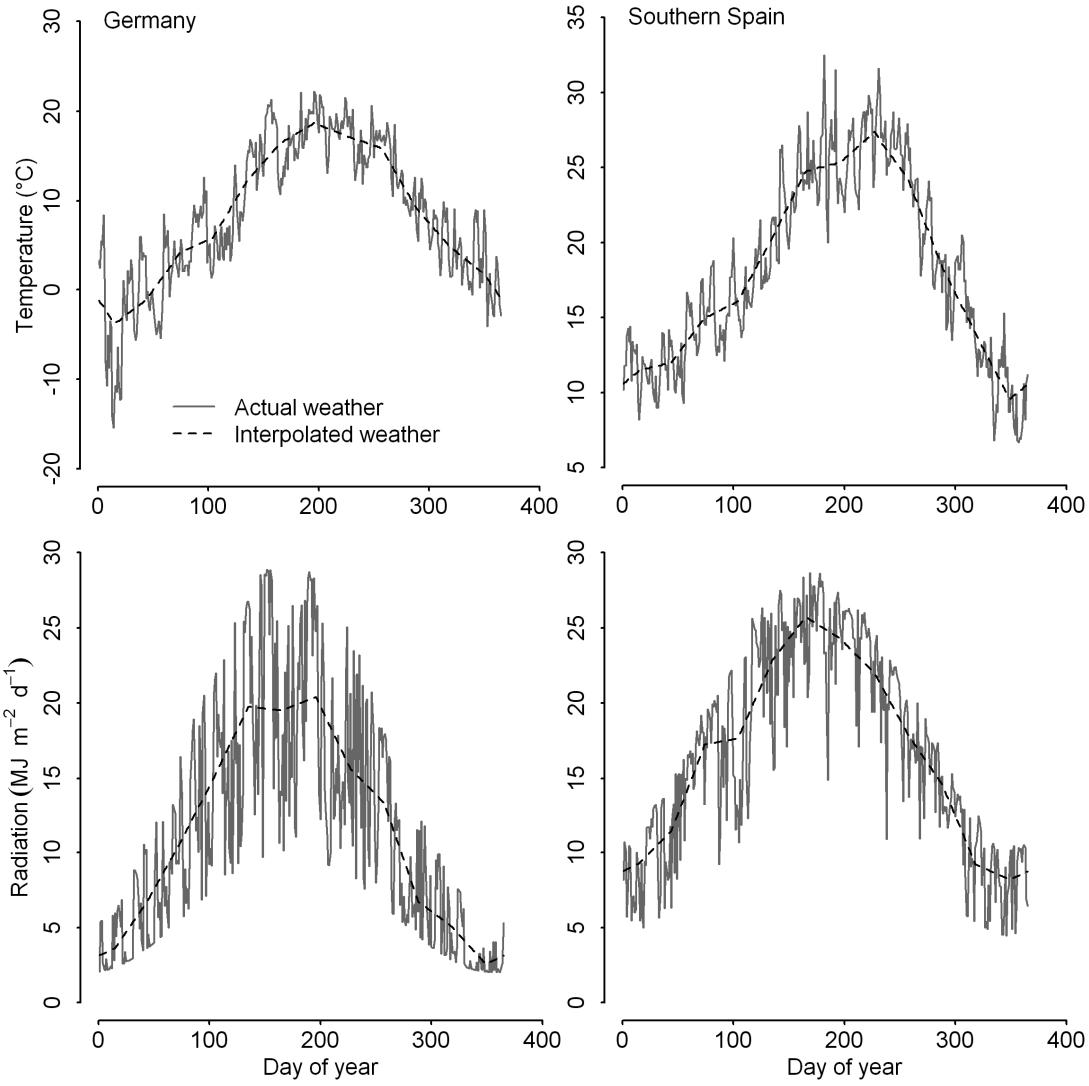

Figure 5: Actual and interpolated (daily) temperature (°C) and radiation (MJ m−2 d−1) from weather stations in Germany and southern Spain in 1982.

During the ten days following anthesis, actual daily $T_{\max}$ exceeded at least during one day the threshold temperature of 27°C in all locations, except those in the United Kingdom and in central France. In the Netherlands, southern France, Spain, and Italy, actual daily $T_{\max}$ also exceeded at least once the threshold temperature of 31°C in the ten days following anthesis. If interpolated daily $T_{\max}$ data were used, only in southern France, Spain, and Italy $T_{\max}$ exceeded 27°C, $T_{\max}$ never exceeded 31°C. However, $T_{\max}$

exceeded 27°C on more days if interpolated daily $T_{\max}$ was used than with actual daily $T_{\max}$. Daily T_{average} (actual and interpolated) never exceeded 27°C during the ten days following anthesis (Table 4).

Number of days when $T_{\max}$ exceeded a certain threshold temperature for two input data sets; T_{average} (actual daily and interpolated daily) never exceeded 27°C.

Table 4: Number of days when $T_{\max}$ exceeded a certain threshold temperature for two input data sets; T_{average} (actual daily and interpolated daily) never exceeded 27°C.

Location	Days with actual daily $T_{\max}$ above		Days with interpolated daily $T_{\max}$ above	
	27°C	31°C	27°C	31°C
United Kingdom	0	0	0	0
Denmark	2	0	0	0
the Netherlands	4	1	0	0
Germany	1	0	0	0
France (centre)	0	0	0	0
France (south)	5	1	3	0
Spain (centre)	9	3	10	0
Spain (south)	6	3	10	0
Italy	6	2	10	0

3.2. Total biomass for actual and linearly interpolated weather data

Sensitivity of the different model combinations to interpolation of input data was tested for interpolation of temperature and radiation separately and for the combination of both interpolated temperature and radiation. Figure 6 shows the average (relative) differences between simulated total standing biomass with actual weather data and with interpolated weather data based on the nine stations (see Eq. 1), for irrigated and rainfed conditions.

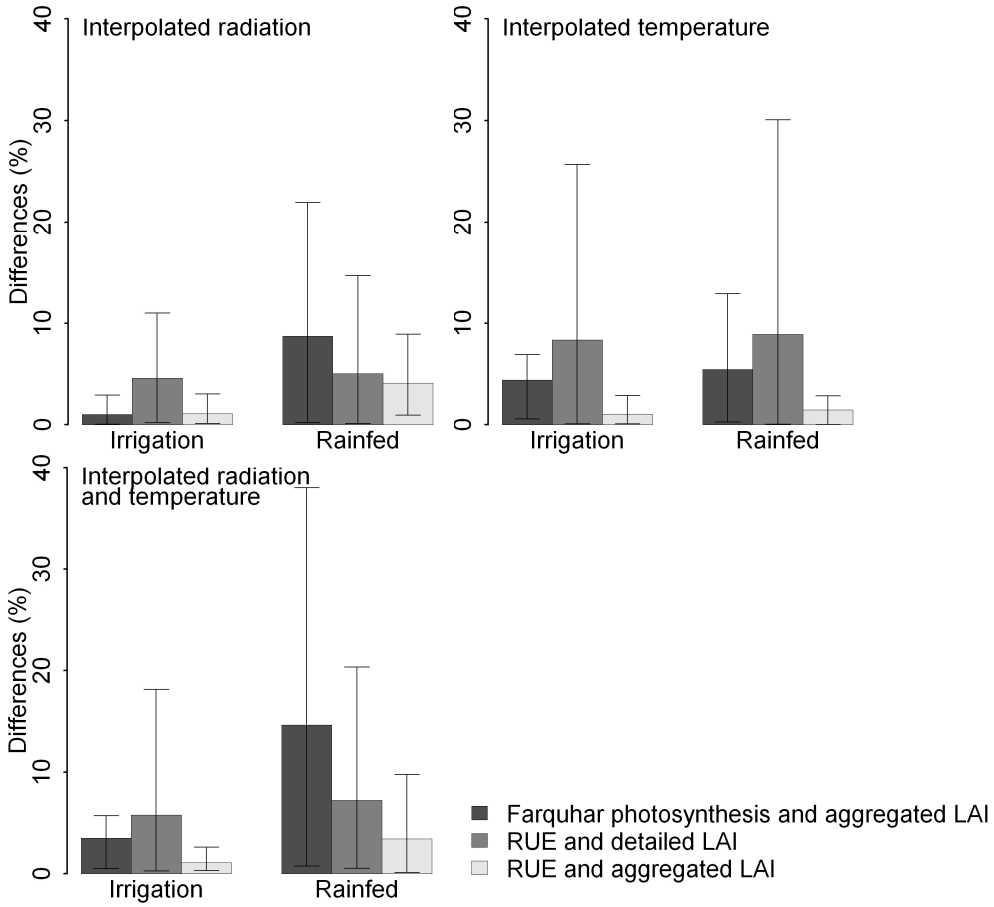

Figure 6: Average differences (%) based on all nine locations in simulated total biomass at the end of the growing season, using "actual temperature and actual radiation" compared to the use of interpolated data, for irrigated and rainfed conditions. The error bars indicate the maximum and minimum differences.

FIGURE 7

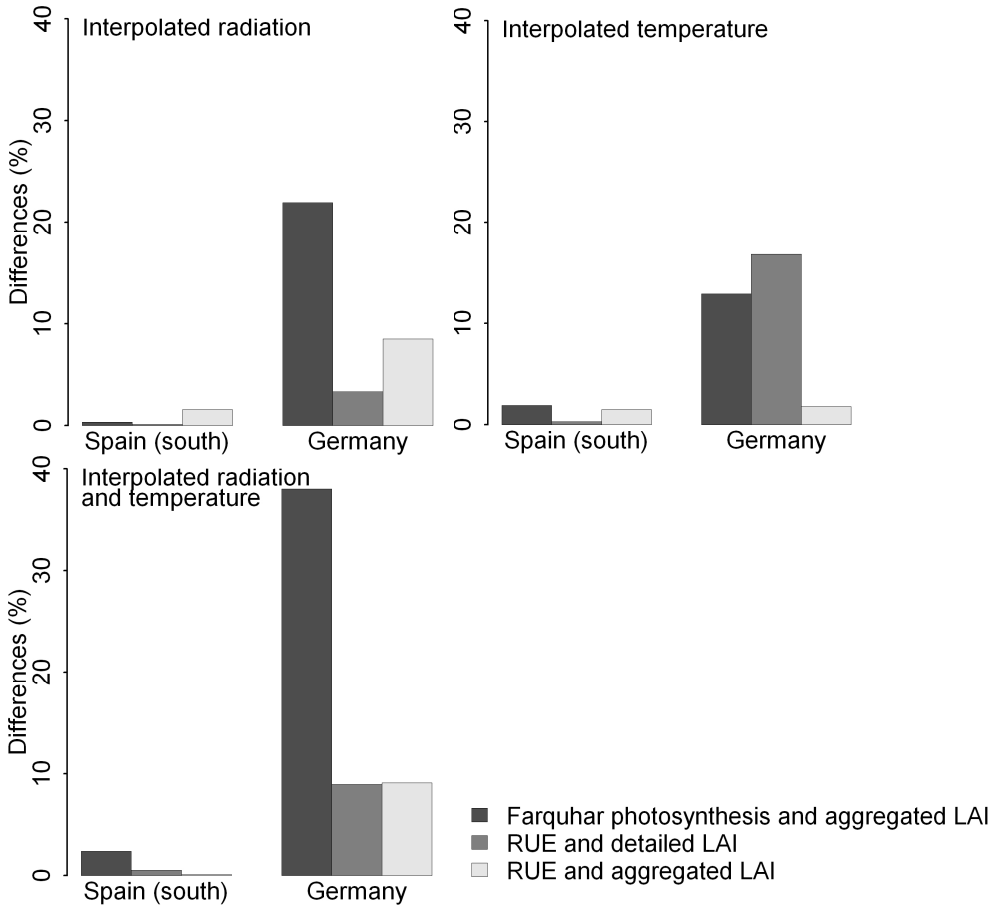

Figure 7: Differences (%) in simulated total biomass at the end of the growing season using "actual temperature and actual radiation" compared to the use of interpolated data for southern Spain and Germany for rainfed conditions.

The models respond differently to the interpolation of the different types of input data. Differences under rainfed conditions are in general larger than under irrigated conditions, especially for the combination of both interpolated radiation and temperature. Using the Farquhar photosynthesis model with the summarized LAI approach, under rainfed conditions, results in an average difference of 15% (averaged over the nine stations, Fig. 6) in simulated total biomass between simulations with actual and simulations with the combination of both interpolated temperature and radiation, with a maximum

of 38% in Germany (Fig. 7). Using the RUE approach combined with the detailed LAI approach, under rainfed conditions, results in an average difference of 9% between simulations with actual and simulations with interpolated temperature and actual radiation data, with a maximum of 30% in the UK. The most summarized combination (RUE and summarized LAI approach), under rainfed conditions, results in the lowest average difference (4%) between simulations with actual and those with actual temperature and interpolated radiation, with a maximum of 9% in Denmark.

The effects vary among locations as shown for two contrasting locations: southern Spain and Germany (Fig. 7). Locations with a low day-to-day variability in weather conditions, such as southern Spain, show small differences as a result of the use of interpolated temperature and/or radiation data, for both irrigated and rainfed conditions. In contrast, locations with a high day-to-day variability, such as Germany, especially the use of the Farquhar photosynthesis approach results in large differences of up to 37%, if interpolated data for both temperature and radiation are used (Fig. 7). In Fig. 8 we show the relationship between the day-to-day variability in weather variables (see Eq. 3), and the difference between model results with actual and interpolated weather data (see Eq. 1), for the model combination with the detailed biomass model (Fig 1c). It is evident that for this model combination a systematic positive linear relationship exists, i.e. a higher day-to-day variability in weather conditions results in a larger difference in biomass production between input data sets. Relationships between day-to-day-variability in

weather conditions and differences in simulation results for the other combinations of approaches are less distinct (not shown).

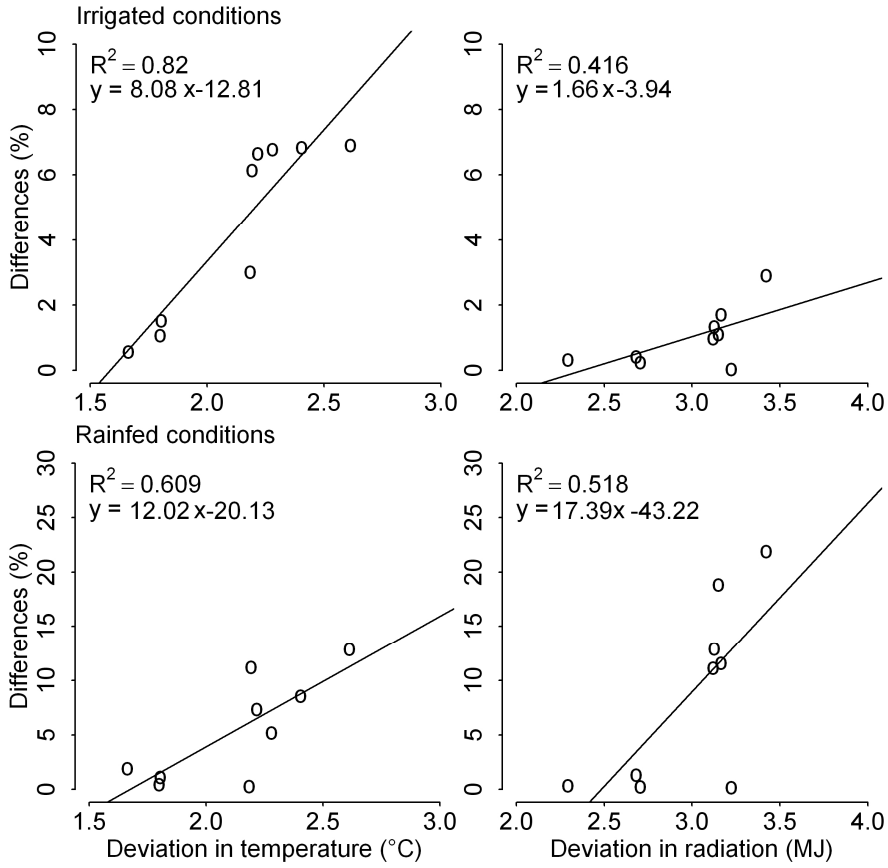

Figure 8: Relation between the average annual difference between actual and interpolated weather data on the one hand (x-axis, indicating the magnitude of the day-to-day variability of the weather variables, Eq. 3), and the difference between model runs driven by actual and interpolated weather data on the other hand (y-axis, Eq. 1); for the combination of the Farquhar photosynthesis and the summarized leaf area index approach.

The use of aggregated temperature data results for several stations in a small change in the timing of anthesis and in at most one day change in the simulated length of the growing season. Therefore, differences in simulated biomass are not attributable to simulated differences in length of the growing period, but are almost exclusively due to weather variability during the growing period.

4. Discussion and conclusions

The objective of this study was to analyse the sensitivity of crop modelling approaches, representing growth processes, with different detail, in response to changes in the temporal resolution of weather input data. Our results show that the simulated biomass depends on whether actual or interpolated temperature and/or radiation data are used. This is in line with earlier results of Nonhebel (1994) and Soltani et al. (2004). Nonhebel (1994) studied locations with high day-to-day variability in weather conditions and found overestimates of 5 – 15% for simulated potential yields as a result of using average weather data. Soltani et al. (2004) found significant over-estimates of yield with linearly interpolated input data at the locations with optimal or supra optimal air temperatures for crop growth and a high day-to-day variability. Importantly, in the present study, we find in addition, that the sensitivity to the interpolation of input data not only depends on the magnitude of the day-to-day weather variability, but also increases with increasing detail in the process modelling. For the most summarized model combination, the difference at a particular site between simulated biomass with actual and simulated biomass with linearly interpolated input data is at most 10%, while for the most detailed model combination it is 37%.

The large differences (higher simulated biomass with aggregated weather data) in the model with the Farquhar photosynthesis approach can be explained by the nonlinear temperature effect on the assimilation rate incorporated in that approach (Fig. 3). Due to the lack of day-to-day variability in linearly interpolated weather data, temperatures are more often at or near optimum values for growth, resulting in higher photosynthetic rates. In

contrast, the more linear nature of the other approaches resulted in smaller differences. Furthermore, we found for the Farquhar photosynthesis approach a positive linear relationship between the day-to-day variability in weather conditions and the differences in simulated biomass between simulations driven with actual and with linearly interpolated input data (Fig 8). This indicates that in locations with high day-to-day variability in weather conditions, and therefore large differences between actual and linearly interpolated weather data, differences due to the use of linearly interpolated input data are large.

The required structure, parameter values and input data for a model to assess effects of extreme weather events, e.g. heat waves, on crop growth are not yet fully understood. Existing models that include these effects, often apply threshold approaches, as e.g. $T_{\max}$ thresholds for heat stress (Challinor et al., 2005; Teixeira et al., 2010). Our results, however, suggest that current threshold models cannot be simply applied with temporally aggregated weather data, if calibrated with more detailed weather data. We cannot conclude that threshold models are generally unsuitable in combination with aggregated data, but at least current threshold values will have to be re-parameterized if weather data with different characteristics (interpolated vs. actual; mean vs. maximum) are being used. Furthermore, whether threshold temperature models for heat damage to crops can be applied with interpolated monthly data also largely depends on the local day-to-day temperature variability and their statistical distribution characteristics. An in-depth analysis

of a global set of daily temperature measurements would be required, which is beyond the scope of this study.

In addition to heat stress, effects such as yield reductions due to ozone pollution are also simulated using threshold values (e.g. Ewert and Porter, 2000). This effect has not been considered here, as it is not addressed in any global-scale crop growth model, however, it is likely that re-parameterization is also advisable if input data with a different temporal resolution are being used, than that applied in the original model.

Based on the results presented here, we stress the importance of the provision of daily weather data. Such data may be generated through weather generators, in combination with or directly by global circulation models. However, site-specific observed daily weather data, which are often required to calibrate weather generators, are currently unavailable for large parts of the Earth (Liu et al., 2009), which hampers the application of weather generators at the global scale. For that reason, we stress that observed daily weather data should be made available for more regions and measurement sites. Results of weather generators should be tested for various climates, especially for climates with extreme temperatures, in order to assess their applicability in climate impact assessments, which may require rather detailed crop growth models, at least for conditions of high day-to-day weather variability.

Our hypothesis that model sensitivity to the use of temporally aggregated data increases with an increasing degree of detail in the modelling approach, is supported by the results of this study. This observation has implications for

the choice of a specific approach to model a certain process, which thus depends on the temporal resolution of the available input data. However, whether model uncertainty is unnecessarily increased if detailed approaches are combined with temporarily sparse weather data, needs further evaluation. Nevertheless, we suggest that the available temporal resolution of the input data and the implications for model results and model applicability need to be taken into account in the design of a (global) crop growth model. More detailed models need to be (re-)evaluated or re-parameterised if driven with less detailed input data, while more summarized models may prove to be unsuitable for studies addressing the effects of changes in day-to-day weather patterns, such as studies on weather extremes.

Acknowledgements

The authors are grateful for the valuable comments of two anonymous reviewers, who proposed useful revisions to a previous version of this paper.

References

Adam, M., Van Bussel, L.G.J., Leffelaar, P.A., Van Keulen, H. and Ewert, F., under review. Effects of modelling detail on simulated crop productivity under a wide range of climatic conditions. Ecol. Model.

Apipattanavis, S., Bert, F., Podestá, G. and Rajagopalan, B., 2010. Linking weather generators and crop models for assessment of climate forecast outcomes. Agric. For. Meteorol. 150, 166-174.

Battisti, D.S. and Naylor, R.L., 2009. Historical warnings of future food insecurity with unprecedented seasonal heat. Science 323, 240-244.

Beniston, M., Stephenson, D.B., Christensen, O.B., Ferro, C.A.T., Frei, C., Goyette, S., Halsnaes, K., Holt, T., Jylhä, K., Koffi, B., Palutikof, J., Schöll, R., Semmler, T. and Woth, K., 2007. Future extreme events in European climate: an exploration of regional climate model projections. Clim. Change 81, 71-95.

Bondeau, A., Smith, P.C., Zaehle, S., Schaphoff, S., Lucht, W., Cramer, W., Gerten, D., Lotze-Campen, H., Müller, C., Reichstein, M. and Smith, B., 2007. Modelling the role of agriculture for the 20th century global terrestrial carbon balance. Glob. Change Biol. 13, 679-706.

Challinor, A.J., Wheeler, T.R., Craufurd, P.Q., Slingo, J.M. and Grimes, D.I.F., 2004. Design and optimisation of a large-area process-based model for annual crops. Agric. For. Meteorol. 124, 99-120.

Challinor, A.J., Wheeler, T.R., Craufurd, P.Q. and Slingo, J.M., 2005. Simulation of the impact of high temperature stress on annual crop yields. Agric. For. Meteorol. 135, 180-189.

Collatz, G.J., Ball, J.T., Grivet, C. and Berry, J.A., 1991. Physiological and

environmental regulation of stomatal conductance, photosynthesis and transpiration: a model that includes a laminar boundary layer. Agric. For. Meteorol. 54, 107-136.

Easterling, D.R., Meehl, G.A., Parmesan, C., Changnon, S.A., Karl, T.R. and Mearns, L.O., 2000. Climate extremes: observations, modeling, and impacts. Science 289, 2068-2074.

Ewert, F., Van Oijen, M. and Porter, J.R., 1999. Simulation of growth and development processes of spring wheat in response to CO_2 and ozone for different sites and years in Europe using mechanistic crop simulation models. Eur. J. Agron. 10, 231-247.

Ewert, F. and Porter, J., R., 2000. Ozone effects on wheat in relation to CO_2: modelling short-term and long-term responses of leaf photosynthesis and leaf duration. Glob. Change Biol. 6, 735-750.

Ewert, F., 2004. Modelling changes in global regionalized food production systems under changing climate and consequences for food security and environment – development of an approach for improved crop modelling within IMAGE. Plant Production Systems Group, Department of Plant Sciences, Wageningen University & Netherlands Environmental Assessment Agency (MNP), National Institute for Public Health and Environment (RIVM).

Ewert, F., Rounsevell, M.D.A., Reginster, I., Metzger, M.J. and Leemans, R., 2005. Future scenarios of European agricultural land use: I. estimating changes in crop productivity. Agric. Ecosyst. Environ. 107, 101-116.

Farquhar, G.G., von Caemmerer, S. and Berry, J.A., 1980. A biochemical

model of photosynthetic CO_2 assimilation in leaves of C3 species. Planta 149, 78-90.

Farré, I., Van Oijen, M., Leffelaar, P.A. and Faci, J.M., 2000. Analysis of maize growth for different irrigation strategies in northeastern Spain. Eur. J. Agron. 12, 225-238.

Ferris, R., Ellis, R.H., Wheeler, T.R. and Hadley, P., 1998. Effect of high temperature stress at anthesis on grain yield and biomass of field-grown crops of wheat. Ann. Bot. 82, 631-639.

Gabrielle, B., Denoroy, P., Gosse, G., Justes, E. and Andersen, M.N., 1998. A model of leaf area development and senescence for winter oilseed rape. Field Crops Res. 57, 209-222.

Gerten, D., Schaphoff, S., Haberlandt, U., Lucht, W. and Sitch, S., 2004. Terrestrial vegetation and water balance – hydrological evaluation of a dynamic global vegetation model. J. Hydrol. 286, 249-270.

Goudriaan, J. and Monteith, J.L., 1990. A mathematical function for crop growth based on light interception and leaf area expansion. Ann. Bot. 66, 695-701.

Hammer, G.L., Kropff, M.J., Sinclair, T.R. and Porter, J.R., 2002. Future contributions of crop modelling – from heuristics and supporting decision making to understanding genetic regulation and aiding crop improvement. Eur. J. Agron. 18, 15-31.

Hansen, J.W., Challinor, A., Ines, A., Wheeler, T. and Moron, V., 2006. Translating climate forecasts into agricultural terms: advances and challenges. Clim. Res. 33, 27-41.

Haxeltine, A. and Prentice, I.C., 1996. BIOME3: An equilibrium terrestrial

biosphere model based on ecophysiological constraints, resource availability, and competition among plant functional types. Glob. Biogeochem. Cycles 10, 693-709.

Hirabayashi, Y., Kanae, S., Motoya, K., Masuda, K. and Döll, P., 2008. A 59 year (1948-2006) global near-surface meteorological data set for land surface models. Part I: development of daily forcing and assessment of precipitation intensity. Hydrol. Res. Lett. 2, 36-40.

Irmak, A., Jones, J.W. and Jagtap, S.S., 2005. Evaluation of the CROPGRO soybean model for assessing climate impacts on regional soybean yields. Trans. ASAE 48, 2343-2353.

Leemans, R., 1997. Effects of global change on agricultural land use: scaling up from physiological processes to ecosystem dynamics, in: Jackson, L.E. (Ed.), Ecology in Agriculture. Academic Press, San Diego, pp. 415-452.

Liu, J., Williams, J.R., Zehnder, A.J.B. and Yang, H., 2007. GEPIC – modelling wheat yield and crop water productivity with high resolution on a global scale. Agric. Syst. 94, 478-493.

Liu, J., Williams, J.R., Wang, X. and Yang, H., 2009. Using MODAWEC to generate daily weather data for the EPIC model. Environ. Model. Softw. 24, 655-664.

LLNL, http://www-pcmdi.llnl.gov/ (Accessed 8 July 2009).

Long, S.P. and Ort, D.R., 2010. More than taking the heat: crops and global change. Curr. Opin. Plant Biol. 13, 240-247.

Mitchell, R.A.C., Mitchell, V.J., Driscoll, S.P., Franklin, J. and Lawlor, D.W.,

1993. Effects of increased CO_2 concentration and temperature on growth and yield of winter wheat at two levels of nitrogen application. Plant Cell Environ. 16, 521-529.

Monteith, J.L., 1977. Climate and efficiency of crop production in Britain. Phil. Trans. R. Soc. Lond. B 281, 277-294.

Monteith, J.L., 2000. Agricultural meteorology: evolution and application. Agric. For. Meteorol. 103, 5-9.

Neitsch, S.L., Arnold, J.G., Kiniry, J.R. and Williams, J.R., 2005. Soil and water assessment tool theoretical documentation, version 2005, USDA-ARS-SR Grassland, Soil and Water Research Laboratory, Agricultural Research Service, Temple, Texas, US.

Nonhebel, S., 1994. The effects of use of average instead of daily weather data in crop growth simulation models. Agric. Syst. 44, 377-396.

Penman, H.L., 1948. Natural evaporation from open water, bare soil and grass. Proc. R. Soc. Lond. 193, 120-146.

Porter, J.R. and Gawith, M., 1999. Temperatures and the growth and development of wheat: a review. Eur. J. Agron. 10, 23-36.

Porter, J.R. and Semenov, M.A., 2005. Crop responses to climatic variation. Phil. Trans. R. Soc. Lond. B 360, 2021-2035.

Reidsma, P., Ewert, F., Boogaard, H. and Van Diepen, K., 2009. Regional crop modelling in Europe: the impact of climatic conditions and farm characteristics on maize yields. Agric. Syst. 100, 51-60.

Saini, H.S. and Aspinall, D., 1982. Abnormal sporogenesis in wheat (*Triticum aestivum* L.) induced by short periods of high temperature. Ann. Bot. 49, 835-846.

Salinger, M., Sivakumar, M.V.K. and Motha, R., 2005. Reducing vulnerability of agriculture and forestry to climate variability and change: workshop summary and recommendations. Climatic Change 70, 341-362.

Semenov, M.A. and Porter, J.R., 1995. Climatic variability and the modeling of crop yields. Agric. For. Meteorol. 73, 265-283.

Semenov, M.A., 2009. Impacts of climate change on wheat in England and Wales. J. R. Soc. Interface 6, 343-350.

Sheffield, J., Goteti, G. and Wood, E.F., 2006. Development of a 50-year high resolution global dataset of meteorological forcings for land surface modeling. J. Clim. 19, 3088-3111.

Sitch, S., Smith, B., Prentice, I.C., Arneth, A., Bondeau, A., Cramer, W., Kaplan, J.O., Levis, S., Lucht, W., Sykes, M.T., Thonicke, K. and Venevsky, S., 2003. Evaluation of ecosystem dynamics, plant geography and terrestrial carbon cycling in the LPJ dynamic global vegetation model. Glob. Change Biol. 9, 161-185.

Soltani, A., Meinke, H. and De Voil, P., 2004. Assessing linear interpolation to generate daily radiation and temperature data for use in crop simulations. Eur. J. Agron. 21, 133-148.

Soussana, J.-F., Graux, A.-I. and Tubiello, F.N., 2010. Improving the use of modelling for projections of climate change impacts on crops and pastures. J. Exp. Bot. 61, 2217-2228.

Spitters, C.J.T. and Schapendonk, A., 1990. Evaluation of breeding strategies for drought tolerance in potato by means of crop growth simulation. Plant Soil 123, 193-203.

Stehfest, E., Heistermann, M., Priess, J.A., Ojima, D.S. and Alcamo, J., 2007.

Simulation of global crop production with the ecosystem model DayCent. Ecol. Model. 209, 203-219.

Teixeira, E., Fischer, G., Ewert, F., Van Velthuizen, H., Challinor, A. and Walter, C., 2010. Hot-spots of heat-stress damage for rice and wheat crops due to climate change, Conference Proceedings, XI ESA Congress, Montpellier, France.

Tubiello, F.N. and Fischer, G., 2007. Reducing climate change impacts on agriculture: global and regional effects of mitigation, 2000-2080. Technol. Forecast. Soc. 74, 1030-1056.

Van Delden, A., Kropff, M.J. and Haverkort, A.J., 2001. Modeling temperature- and radiation-driven leaf area expansion in the contrasting crops potato and wheat. Field Crops Res. 72, 119-141.

Van Ittersum, M.K., Leffelaar, P.A., Van Keulen, H., Kropff, M.J., Bastiaans, L. and Goudriaan, J., 2003. On approaches and applications of the Wageningen crop models. Eur. J. Agron. 18, 201-234.

Van Kraalingen, D.W.G., Stol, W., Uithol, P.W.J. and Verbeek, M.G.M., 1991. User manual of CABO/TPE Weather System, WAU-TPE, Wageningen.

Van Oijen, M. and Ewert, F., 1999. The effects of climatic variation in Europe on the yield response of spring wheat cv. Minaret to elevated CO_2 and O^{-3}: an analysis of open-top chamber experiments by means of two crop growth simulation models. Eur. J. Agron. 10, 249-264.

Yin, X., Schapendonk, A.H.C.M., Kropff, M.J., Van Oijen, M. and Bindraban, P.S., 2000. A generic equation for nitrogen-limited leaf area index and its application in crop growth models for predicting leaf senescence. Ann. Bot. 85, 579-585.

Appendix

1. Radiation interception

1.1. Detailed leaf area index approach

During the juvenile stage or until a certain LAI threshold ($LAI_{\text{juvenile stage}}$, m^2 m^{-2}), the rate of increase of LAI is exponential and mainly driven by temperature, through its effect on cell division and extension:

$$\frac{\mathrm{d}LAI}{\mathrm{d}t} = LAI \times R_{\mathrm{g}} \times T_{\mathrm{eff}} \times W_{\mathrm{f}} \tag{A.1}$$

$$T_{\mathrm{eff}} = \max(0, [T_{\mathrm{average}} - T_{\mathrm{base}}]) \tag{A.2}$$

where, R_{g} ((°Cd) $^{-1}$) is the maximum relative growth rate of LAI, T_{eff} (°C) the effective temperature, calculated as the difference between daily average temperature (T_{average}, °C) and a base temperature (T_{base}, °C), and W_{f} (–) a water stress factor, derived from the ratio between actual and potential transpiration.

Beyond the juvenile stage:

$$\frac{\mathrm{d}LAI}{\mathrm{d}t} = \frac{\mathrm{d}W_{\mathrm{l}}}{\mathrm{d}t} \times S_{\mathrm{LA}} \times W_{\mathrm{f}} \tag{A.3}$$

where, $\mathrm{d}W_{\mathrm{l}}/\mathrm{d}t$ (g C m^{-2} d^{-1}) is the simulated rate of increase in leaf weight and S_{LA} (m^2 (g C)$^{-1}$) is a constant specific leaf area of new leaves.

The senescence rate is described by:

$$\frac{\mathrm{d}LAI}{\mathrm{d}t} = -r_{\mathrm{d}} \times LAI \tag{A.4}$$

with:

$$r_{\mathrm{d}} = \max\left(R_{\text{d-ag}}, R_{\text{d-sh}}\right) \text{ and} \tag{A.5}$$

$$R_{\text{d-sh}} = \max\left[0, \min\left(R_{\text{d-shmx}}, R_{\text{d-shmx}} \times \frac{LAI - LAI_{\mathrm{c}}}{LAI_{\mathrm{c}}}\right)\right] \tag{A.6}$$

where, $R_{\text{d-ag}}$ is an exogenously defined relation between temperature and the relative death rate due to ageing (Fig. 2), which only takes place after anthesis. $R_{\text{d-sh}}$ is the relative death rate due to shading, where LAI_{c} (m^2 m^{-2}) is the critical value above which shading only takes place and $R_{\text{d-shmx}}$ (d^{-1}), the maximum possible relative senescence rate due to shading.

1.2.Summarized leaf area index approach

Before senescence starts, the fraction of an exogenously defined maximum leaf area index ($fLAI_{\text{max}}$, –) is calculated as:

$$fLAI_{\text{max}} = \frac{fT_{\text{sum}}}{fT_{\text{sum}} + \exp\left(l_1 - l_2 \times fT_{\text{sum}}\right)} \tag{A.7}$$

$$l_1 = \ln\left(\frac{fT_{\text{sum}_1}}{fLAI_1} - fT_{\text{sum}_1}\right) + l_2 \times fT_{\text{sum}_1} \tag{A.8}$$

$$l_2 = \frac{\ln\left[\frac{fT_{\text{sum}_1}}{fLAI_1} - fT_{\text{sum}_1}\right] - \ln\left[\frac{fT_{\text{sum}_2}}{fLAI_2} - fT_{\text{sum}_2}\right]}{fT_{\text{sum}_2} - fT_{\text{sum}_1}} \tag{A.9}$$

where, fT_{sum} (–) is the fraction, on a specific day, of the total temperature sum required to reach maturity (based on the effective temperature), and l_1 (–) and l_2 (–) are shape coefficients, calculated from the fractions of leaf area index ($fLAI_1$, –; $fLAI_2$, –) and the fractions of the temperature sum (fT_{sum_1}, –; fT_{sum_2}, –) at exogenously defined inflexion points on the leaf area development curve. Following the onset of senescence, $fLAI_{\text{max}}$ is calculated as:

$$fLAI_{\text{max}} = \frac{(1 - fT_{\text{sum}})^2}{(1 - fT_{\text{sum a}})^2} \tag{A.10}$$

where, $fT_{\text{sum a}}$ (–) is the fraction of the total temperature sum when senescence starts.

Potential leaf area index (LAI_{p}, $m^2\ m^{-2}$) is calculated from an exogenously defined crop-specific maximum leaf area index ($LAI_{\max}$, $m^2\ m^{-2}$) and $fLAI_{\max}$:

$$LAI_{\mathrm{p}} = fLAI_{\max} \times LAI_{\max} \tag{A.11}$$

LAI_{p} is reduced if the biomass required to support the calculated leaf area index is not available:

$$LAI = \min\left(LAI_{\mathrm{p}}, \left[B_{\mathrm{t}} - B_{\mathrm{r}}\right] \times S_{\mathrm{LA}}\right) \tag{A.12}$$

where, B_{t} and B_{r} (g C m^{-2}) are standing total biomass and standing root biomass, respectively (Bondeau et al., 2007; Neitsch et al., 2005).

To account for water stress, in the pre-anthesis phase a water scaler (W_{s},–) is included to reduce LAI_{p}. This water stress scaler is either based on the ratio of actual and potential transpiration (in combination with the radiation use efficiency approach), or (in combination with the Farquhar photosynthesis model) as follows:

$$W_{\mathrm{s}} = \frac{S}{\left(E_{\mathrm{q}} \times \alpha_{\max}\right) / \left(1 + \frac{g_{\mathrm{m}}}{g_{\mathrm{p}}}\right)} \tag{A.13}$$

where, S is water supply (see Eq. (A.30), mm d^{-1}), $(E_{\mathrm{q}} \times \alpha_{\max})$ potential evapotranspiration (mm d^{-1}), g_{m} a scaling factor (mm s^{-1}), and g_{p} potential canopy conductance (see Eq. (A.29), mm s^{-1}) (Gerten et al., 2004).

2. Biomass productivity

2.1. Detailed biomass productivity approach

Daily net photosynthesis (A_{nd}, g C m^{-2} d^{-1}) is calculated as the gradual transition between the light-limited (J_{e}, g C m^{-2} h^{-1}) and Rubisco-limited (J_{c}, g C m^{-2} h^{-1}) conditions:

$$A_{\mathrm{nd}} = \left(\frac{J_{\mathrm{e}} + J_{\mathrm{c}} - \sqrt{(J_{\mathrm{e}} + J_{\mathrm{c}})^2 - 4 \times \theta \times J_{\mathrm{e}} \times J_{\mathrm{c}}}}{2 \times \theta} \right) \times d_{\mathrm{length}} - R_{\mathrm{d}} \quad \text{(A.14)}$$

where, θ is a co-limitation parameter (–), d_{l} (h d^{-1}) the day length, and R_{d} (g C m^{-2} d^{-1}) the "dark respiration", with:

$$J_{\mathrm{c}} = \frac{C_1 \times APAR \times C_{\mathrm{q}}}{d_{\mathrm{l}}} \quad \text{(A.15)}$$

$$J_{\mathrm{c}} = \frac{C_2 \times V_{\mathrm{m}}}{24} \quad \text{(A.16)}$$

where, $APAR$ (MJ m^{-2} d^{-1}) is daily absorbed photosynthetically active radiation and C_{q} (mol photons MJ^{-1}) a conversion factor for solar radiation, with:

$$C_1 = \phi_{\mathrm{TC3}} \times C_{\mathrm{mass}} \times \alpha_{\mathrm{C3}} \times \frac{p_{\mathrm{i}} - \Gamma_*}{p_{\mathrm{i}} + 2 \times \Gamma_*}, \quad \text{(A.17)}$$

$$C_2 = \frac{p_{\mathrm{i}} - \Gamma_*}{p_{\mathrm{i}} + K_{\mathrm{C}} \times (1 + \frac{[O_2]}{K_{\mathrm{O}}})}, \quad \text{(A.18)}$$

p_{i} (Pa), the partial pressure of CO_2 in the intercellular air spaces of the leaf:

$p_{\mathrm{i}} = \lambda \times c_{\mathrm{a}} \times P$ and (A.19)

p_{a} (Pa), the partial pressure of ambient CO_2:

$$p_{\mathrm{a}} = c_{\mathrm{a}} \times P \quad \text{(A.20)}$$

$\Gamma*$ (Pa), the CO_2 compensation point:

$\Gamma_* = \frac{[O_2]}{2 \times \tau}$, and (A.21)

the temperature dependent parameters K_{C}, K_{O}, and τ:

$$K_{\mathrm{i}} = K_{25} \times Q_{10}^{(T-25)/10} \quad \text{(A.22)}$$

where, the number 24 (h d^{-1}) is the number of hours per day, ϕ_{TC3} (–) a temperature stress factor, C_{mass} (g mol^{-1}) the atomic mass of carbon, α_{C3} the C3 quantum efficiency (µmol µmol^{-1}), $[O_2]$ (Pa) the partial pressure of oxygen,

λ (Pa Pa^{-1}) the ratio of p_{i} to p_{a} (λ = $\lambda_{\max}$ under optimal water conditions), c_{a} (µmol mol^{-1}) the ambient mole fraction of CO_2, P atmospheric pressure (Pa), K_{C} (Pa) the Michaelis-Menten constant for CO_2, K_{O} (Pa) the Michaelis-Menten constant for O_2, τ (µmol µmol^{-1}) the CO_2/O_2 specificity ratio, with K_{i} either K_{C}, K_{O} or τ, and Q_{10} the accompanying Q_{10} values, and V_m (g C m^{-2} d^{-1}) the maximum daily rate of photosynthesis:

$$V_{\mathrm{m}} = \left(\frac{1}{b}\right) \times \left(\frac{C_1}{C_2}\right) \times \left[\left(2 \times \theta - 1\right) \times s - \left(2 \times \theta \times s - C_2\right) \times \sigma\right] \times APAR \times C_{\mathrm{q}} \quad \text{(A.23)}$$

with:

$$\sigma = \left[1 - \frac{C_2 - s}{C_2 - \theta \times s}\right]^{1/2}, \quad \text{(A.24)}$$

$$s = \frac{24}{d_{\mathrm{l}}} \times b \text{ , and} \quad \text{(A.25)}$$

the "dark" respiration (R_{d}):

$$R_{\mathrm{d}} = b \times V_{\mathrm{m}} \quad \text{(A.26)}$$

where, b is a constant $R_{\mathrm{d}}/V_{\mathrm{m}}$ ratio (–).

In case of water stress, the photosynthesis rate is related to canopy conductance through the diffusion gradient in CO_2 concentration as a result of the difference in p_{i} and p_{a}. This can be expressed in terms of total daytime net photosynthesis. Total daytime net photosynthesis (A_{dt}, g C m^{-2} d^{-1}) is calculated as:

$$A_{\mathrm{dt}} = A_{\mathrm{nd}} + \left(1 - \frac{d_{\mathrm{l}}}{24}\right) \times R_{\mathrm{d}} \quad \text{(A.27)}$$

Or, expressed in terms of canopy conductance:

$$A_{\mathrm{dt}} = \frac{d_{\mathrm{l}} \times (g_{\mathrm{c}} - g_{\min})}{1.6} \times \left[c_{\mathrm{a}} \times (1 - \lambda)\right] \quad \text{(A.28)}$$

where, g_c (mm s^{-1}) is average daytime canopy conductance, g_{min} (mm s^{-1}) the minimum canopy conductance, which accounts for water loss not directly related with photosynthesis, the factor 1.6 accounts for the difference in the diffusion coefficients of CO_2 and water vapour; in Eq. (A.28) A_{dt} is expressed in mm d^{-1} (the conversion from g C m^{-2} d^{-1} to mm d^{-1} is based on an the ideal gas) and d_l is expressed in s,

g_c is calculated by rearranging Eq. (A.28):

$$g_c = g_{min} + \frac{1.6 \times A_{dt}}{[c_a \times (1 - \lambda)] \times d_l} \quad \text{(A.29)}$$

Maximum (non-water limited) daily net potential photosynthesis rate is calculated with help Eq. (A.28) with $\lambda = \lambda_{max}$, and accordingly, applying Eq. (A.29) and Eq. (A.14) with $\lambda = \lambda_{max}$ and $APAR = PAR$, i.e. all available photosynthetically active radiation, gives the maximum average daytime canopy conductance, i.e. maximum potential canopy conductance (g_p, mm s^{-1}).

Water stress occurs when water supply (S, mm d^{-1}) is lower than water demand (D, mm d^{-1}). Supply is given by the maximum daily transpiration rate possible under well-watered conditions (E_{max}, mm d^{-1}) and the relative soil moisture in the rooting zone (W_r, m^3 m^{-3}):

$$S = E_{max} \times W_r \quad \text{(A.30)}$$

The soil is represented by a simple bucket containing two layers, each with a fixed thickness and a fixed fraction of the roots present. The soil water content of each layer is updated daily, taking into account transpiration, evaporation, runoff, and percolation through the layers. W_r is calculated by summing the

soil water content of the two soil layers, which are multiplied by the fraction of roots in the specific layer and divided by its thickness. Finally, W_{r} is expressed as a fraction of $W_{\max}$, which is a soil-specific parameter, indicating the difference between field capacity and wilting point. Initialisation of the water balance is obtained by a spin-up run (for more details, see Gerten et al., 2004).

Demand is dependent on the fraction of the daytime the canopy is wet (w, –), potential evapotranspiration (($E_{\mathrm{q}} \times \alpha_{\max}$), mm d^{-1}), based on the Priestley-Taylor equations, g_{p}, and an empirical parameter g_{m} (mm s^{-1}):

$$D = (1 - w) \times \frac{(E_{\mathrm{q}} \times \alpha_{\max})}{(1 + \frac{g_{\mathrm{m}}}{g_{\mathrm{pot}}})} \tag{A.31}$$

Water stress results in a lower canopy conductance, therefore, Eqs. (A.20) and (A.33) are solved simultaneously, using a bisection method, to obtain values of A_{nd} and λ under water-limited conditions.

Finally, net primary production (NPP, g C d^{-1} m^{-2}) is calculated as:

$$NPP = A_{\mathrm{nd}} - R_{\mathrm{r}} - R_{\mathrm{so}} - R_{\mathrm{p}} - R_{\mathrm{g}} \tag{A.32}$$

where, R (g C m^{-2} d^{-1}) is the maintenance respiration of roots, storage organs and a reserve pool, respectively, based on tissue-specific C:N ratios, temperature, the amount of biomass, and a respiration rate, and R_{g} the growth respiration:

$$R_{\mathrm{g}} = \max(0, 0.25 \times A_{\mathrm{nd}} - R_{\mathrm{r}} - R_{\mathrm{so}} - R_{\mathrm{p}}) \tag{A.33}$$

A more detailed description of the functions used is provided by Haxeltine and Prentice (1996) and Sitch et al. (2003).

2.2. Summarized biomass productivity approach

Net productivity (NPP, g C m^{-2} d^{-1}) is calculated as:

$$NPP = RUE \times R_{\mathrm{dr}} \times 0.5 \times (1 - e^{-k \times LAI}) \times W_{\mathrm{f}} \quad \text{(A.34)}$$

where, RUE (g C MJ^{-1}) is the radiation use efficiency, R_{dr} (MJ m^{-2} d^{-1}) daily incoming short-wave radiation, and k (–) the light extinction coefficient, the number 0.5 (MJ PAR (MJ short-wave radiation)$^{-1}$) is used, because half of the daily incoming short-wave radiation is photosynthetically active radiation, and W_{f} (–) a water stress factor, i.e. the ratio of actual and potential transpiration. Potential transpiration is calculated based on the Penman equation (Penman, 1948), actual transpiration is calculated based on its potential value, but also on soil water content (W_{c}, m^3 m^{-3}) and soil characteristics. Water available for the crop is calculated on the basis of a soil water balance, calculated for one layer. The thickness of the layer increases with increasing root extension. Newly explored soil is assumed to be at field capacity. Water content of the soil is updated daily, taking into account precipitation, transpiration, evaporation, runoff and percolation. Initial water content, fed into the model, is used for initialisation of the water balance (for more details, see Farré et al., 2000).

Figure captions

Figure 1. Schematic overview of the different model combinations:
a) summarized leaf area index with radiation use efficiency, b) detailed leaf area index with radiation use efficiency, and c) summarized leaf area index with Farquhar photosynthesis.

Figure 2. The relative death rate of leaves (d^{-1}) as a function of temperature (°C), as used in the detailed leaf area index approach.

Figure 3. Temperature response of the daily net rate of photosynthesis, at an ambient CO_2 concentration of 350 ppm and various radiation intensities, as simulated with Farquhar photosynthesis.

Figure 4. Locations of the nine weather stations used in this study.

Figure 5. Actual and interpolated (daily) temperature (°C) and radiation (MJ m^{-2} d^{-1}) from weather stations in Germany and southern Spain in 1982.

Figure 6. Average differences (%) based on all nine locations in simulated total biomass at the end of the growing season, using “actual temperature and actual radiation” compared to the use of interpolated data, for irrigated and rainfed conditions. The error bars indicate the maximum and minimum differences.

Figure 7. Differences (%) in simulated total biomass at the end of the growing season using “actual temperature and actual radiation” compared to the use of interpolated data for southern Spain and Germany for rainfed conditions.

Figure 8. Relation between the average annual difference between actual and interpolated weather data on the one hand (x-axis, indicating the magnitude of the day-to-day variability of the weather variables, Eq. 3), and the difference between model runs driven by actual and interpolated weather data on the other hand (y-axis, Eq. 1); for the combination of the Farquhar photosynthesis and the summarized leaf area index approach.